# Investigation of the Noise Properties of a New Class of Reconstruction Methods in Diffraction Tomography

**Mark A. Anastasio, Xiaochuan Pan**

Department of Radiology, MC-1037, The University of Chicago Medical Center, 5841 S. Maryland Avenue, Chicago, IL 60637

**ABSTRACT:** In diffraction tomography (DT), the measured scattered data are unavoidably contaminated by noise. Because the detectability of an object in a noisy image relies strongly on the signal-to-noise ratio, it is important in certain applications to reduce the statistical variation in the reconstructed image. Recently, we revealed the existence of statistically complementary information inherent in the scattered data and proposed a linear strategy that makes use of this information to achieve a bias-free reduction of the image variance in two-dimensional (2D) DT. This strategy leads to the development of an infinite class of estimation methods, that from the measured scattered data, can estimate the Radon transform of the scattering object function. From the estimated Radon transforms, one can readily reconstruct the object function by using a variety of existing reconstruction algorithms. The estimation methods in the class are mathematically equivalent, but they respond to noise differently. We investigated the noise properties of these estimation methods by use of computer simulation studies. The results of our simulation studies demonstrate quantitatively that it is possible to achieve a bias-free variance reduction in the reconstructed scattering object by utilizing complementary statistical information that is inherent in the scattered data. © 2000 John Wiley & Sons, Inc. Int J Imaging Syst Technol, 10, 437–446, 1999

## I. INTRODUCTION

Diffraction tomography (DT) is a multiview imaging technique that seeks to determine the distribution of the index of refraction of a scattering object. It has found applications in the fields of medical imaging, underwater sound, nondestructive evaluation of materials, and geophysics (Andre et al., 1995; Rouseff and Porter, 1991; Gelius et al., 1991; Langenberg, 1985; Kino, 1979; Robinson, 1984; Mueller et al., 1979). Unlike conventional X-ray computed tomography (CT), the acoustical or electromagnetic radiation in DT is generally treated in terms of wave fields and satisfies the inhomogeneous Helmholtz equation (Ishimaru, 1978; Chernov, 1969; Morse and Ingard, 1986). To obtain the distribution of the scattering object (also referred to as the scattering object function) from the measured scattered data, one needs to invert the inhomogeneous Helmholtz equation. Computationally intensive iterative algorithms are generally required for the exact inversion of the inhomogeneous Helmholtz equation (Chew and Wang, 1990; Lu et al., 1996; Johnson and Tracy, 1983a,b).

When the scattering object is weakly scattering, the Helmholtz equation can be linearized through the use of the Born (or Rytov) approximation (Ishimaru, 1978; Heidbreder, 1967). When the incident radiation is plane-wave, one can derive the Fourier diffraction projection (FDP) theorem (Pan and Kak, 1983; Kaveh et al., 1984; Grassin et al., 1991), which relates the Fourier transform (FT) of the measured scattered fields to the FT of the scattering object function. The FDP theorem provides the basis for reconstruction algorithms such as the filtered back/propagation (FBPP; Devaney, 1982) and direct Fourier (DF) algorithms (Pan and Kak, 1983).

In practice, the measured scattered data are contaminated by noise that arises in the measurement process and from random inhomogeneities in the scattering or background medium. Several researchers have used approaches that are based on the FDP theorem to characterize statistically varying media (Rouseff and Porter, 1991; Fischer and Wolf, 1997). With the exception of the work in reference (Tsihrintzis and Devaney, 1993a), however, it appears that little effort has been devoted to utilizing the statistical information contained in the scattered data to reduce the variance of the reconstructed image. In ultrasonic DT imaging of the female breast, for example, the signal in the image can be subtle. Therefore, it is particularly important to enhance the signal-to-noise ratio, which generally requires that the image variance be reduced. When strong scattering effects are present, linear DT reconstruction algorithms based on the Born or Rytov weak scattering approximations may not produce accurate images. However, many nonlinear DT reconstruction algorithms (Chew and Wang, 1990; Lu et al., 1996) attempt to circumvent the limitations of the Born and Rytov approximations by linearizing the forward scattering problem and solving a linear inverse problem at each step of an iterative procedure. Therefore, in order to properly regularize the nonlinear DT reconstruction problem, it remains important to have an understanding of the noise propagation properties of linear DT reconstruction algorithms.

Recently, we have revealed the existence of statistically complementary information inherent in the scattered data and proposed a linear strategy that makes use of this information to achieve a bias-free reduction of the image variance in two-dimensional (2D) DT (Pan, 1998b). Using this strategy, one can derive infinite classes of estimation methods for obtaining the 2D Radon transform of the scattering object function from the measured scattered data. These estimation methods are mathematically equivalent, but they propagate noise and numerical errors differently (Pan, 1998b). From the

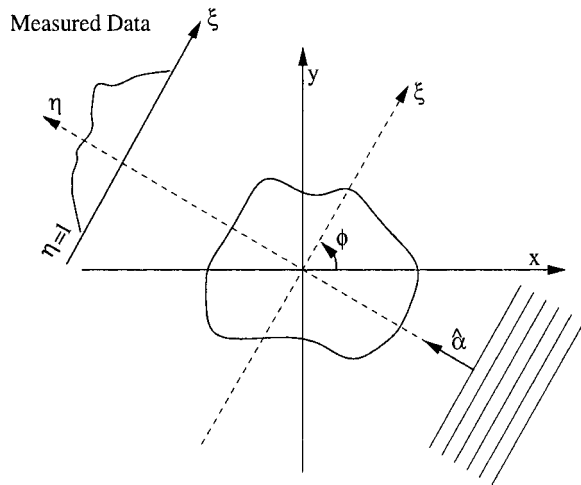*Correspondence to:* M. A. Anastasio; e-mail: anastasi@jedi.bsd.uchicago.edu

**Figure 1.** The classical scan configuration in DT. The incident plane-wave propagates in the $\hat{\alpha}$ direction and the scattered wave field is measured along the line $\eta = l$.

estimated Radon transform, one can readily reconstruct the scattering object function by use of a wide variety of reconstruction algorithms, such as the FBPJ and DF algorithms. The different reconstruction algorithms are mathematically equivalent, but they also respond differently to noise and errors.

In this work, we implemented and evaluated the estimation methods for obtaining the Radon transform of the scattering object function. From these estimated Radon transforms, we reconstructed the scattering object functions by using the FBPJ or DF algorithm. (It should be noted that, as described below, the DF algorithm investigated in this paper differs from the conventional DF algorithm that involves a 2D interpolation.) Therefore, each reconstructed scattering object function is obtained from the scattered data by use of a combination of an estimation method and a reconstruction algorithm. We conducted computer simulations to investigate noise properties of the scattering object functions obtained with different combinations of the estimation methods and reconstruction algorithms. The results of our numerical studies demonstrated quantitatively that the reconstructed scattering object functions are virtually identical in the absence of noise but are noticeably different in the presence of noise, confirming our theoretical assertions. For each reconstruction algorithm, we identified the estimation method that minimizes the global image variance when the scattered data contain uncorrelated Gaussian noise with constant variance.

The paper is organized as follows. Section II discusses the estimation methods for obtaining the Radon transform of the scattering object function from the scattered data in DT and briefly reviews the algorithms for reconstruction of the scattering object function from the estimated Radon transform. Section III describes the simulation studies, including the noise model employed. Section IV presents the results of our numerical simulations such as the calculated image variances obtained with different combinations of estimation methods and reconstruction algorithms. Section V discusses the significance of the results and topics for future work.

## II. THEORY

### A. Basic Formulation of 2D DT.
The classical geometry used in 2D DT is shown in Figure 1. A scattering object is placed in a lossless and homogeneous background medium and is illuminated by monochromatic plane-wave radiation with complex amplitude $U_0$ and frequency $\nu_0$, propagating along the $\eta$-axis. The total field measured along the line $\eta = l$ with an orientation angle $\phi$ can be written as a sum of the incident plane-wave field $u_i(\xi, \phi)$ and the scattered wave field $u_s(\xi, \phi)$. The task in DT is to determine a scattering object function $a(r, \theta)$, using the transmission data measured at various angles about the object. The underlying physical property of the scattering object that is mapped in DT is the refractive index distribution $n(r, \theta)$, which is related to the scattering object function by the equation $a(r, \theta) = n^2(r, \theta) - 1$.

Let $U_s(\nu_m, \phi) = \int_{-\infty}^{\infty} u_s(\xi, \phi)e^{-j2\pi\nu_m\xi}d\xi$ be the 1D FT of the scattered wave field with respect to $\xi$, and let $M(\nu_m, \phi)$ be a modified version of $U_s(\nu_m, \phi)$, which is given by

$$M(\nu_m, \phi) = U_s(\nu_m, \phi)\frac{j\nu'}{2\pi^2\nu_0^2 U_0}e^{-j2\pi\nu'l}, \quad (1)$$

where $\nu' = \sqrt{\nu_0^2 - \nu_m^2}$. Then, under the Born approximation (i.e., $|u_s| \ll |u_i|$), one can obtain a relationship between $M(\nu_m, \phi)$ and $a(r, \theta)$ that can be expressed as

$$
\begin{aligned}
M(\nu_m, \phi) &= \int_{-\infty}^{\infty}\int_{-\infty}^{\infty} a(\vec{r})e^{-j2\pi[\nu_m\xi+(\nu'-\nu_0)\eta]}d\vec{r} \quad \text{if}\,|\nu_m| \leq \nu_0 \\
&= 0 \quad\quad\quad\quad\quad\quad\quad\quad\quad\quad\quad\quad \text{if}\,|\nu_m| > \nu_0,
\end{aligned}
\quad (2)
$$

where the polar coordinates $(r, \theta)$ and rotated coordinates $(\xi, \eta)$ are related through $\xi = r\cos(\phi - \theta)$ and $\eta = -r\sin(\phi - \theta)$. Equation (2), referred to as the FDP theorem (Pan and Kak, 1983), states that the modified FT of the scattered data in Eq. (1) gives the values of the 2D FT of the scattering object function along a semicircular arc of radius $\nu_0$ (Fig. 2).

### B. The Radon transform and Scattered Data.
The Radon transform (Barrett, 1984) of the scattering object function $a(r, \theta)$ is given by
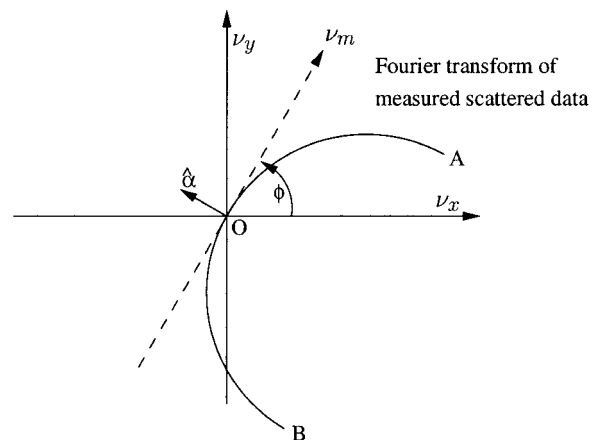


**Figure 2.** The FT of the data measured along the line $\eta = l$ is mapped to a semicircle of radius $\nu_0$ in the Fourier space $\{\nu_x, \nu_y\}$, where $\nu_x$ and $\nu_y$ are the spatial frequencies of $x$ and $y$, respectively.
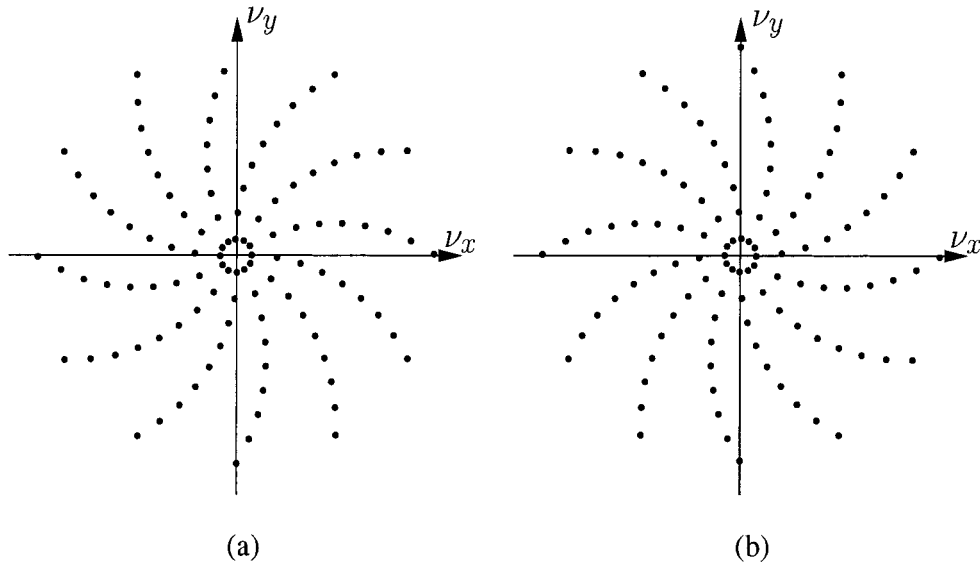
**Figure 3.** Sampling Fourier domain coverages obtained in a DT experiment. (a) Coverage produced by the arc OA. (b) Coverage produced by the arc OB.

$$p(\xi, \phi_0) = \frac{1}{2\pi} \int_{-\infty}^{\infty} \int_{-\infty}^{\infty} a(r, \theta)\delta(\xi - r\cos(\phi_0 - \theta))d\vec{r},$$

$$(3)$$

where $\phi_0$ is the projection angle, $\xi = r\cos(\phi_0 - \theta)$, and $\eta = -r\sin(\phi_0 - \theta)$. It is important to note that the arguments of the function $p(\xi, \phi_0)$ are not the familiar polar coordinates, but rather define a 2D space spanning the range of the Radon transform. The image $a(r, \theta)$ can be reconstructed exactly from its Radon transform $p(\xi, \phi_0)$ by use of a wide variety of computationally efficient and numerically stable reconstruction algorithms, such as the FBPJ and DF algorithms.

The 2D FT of $p(\xi, \phi_0)$ is defined as

$$P(\nu_a, k) = \frac{1}{2\pi} \int_0^{2\pi} \int_{-\infty}^{\infty} p(\xi, \phi_0)e^{-j2\pi\nu_a\xi}e^{-jk\phi_0} \, d\xi \, d\phi_0, \quad (4)$$

where $\nu_a$ is the spatial frequency with respect to $\xi$, and the integer $k$ is the angular frequency index with respect to $\phi_0$. The angular frequency index $k$ is discrete because $p(\xi, \phi_0)$ is periodic in $\phi_0$. In this context, "the 2D FT" we refer to is, in fact, a combination of a 1D FT and a 1D Fourier series expansion. From $P(\nu_a, k)$, one can readily obtain the Radon transform $p(\xi, \phi_0)$ by invoking the 2D inverse FT. Therefore, the task of estimating $p(\xi, \phi_0)$ is equivalent to estimating its 2D FT $P(\nu_a, k)$. Also, it can be shown that the object function $a(r, \theta)$ can be reconstructed from knowledge of $P(\nu_a, k)$ with $\nu_a \geq 0$. Therefore, we will focus only on estimating $P(\nu_a, k)$ for $\nu_a \geq 0$.

It was shown (Pan, 1998b) that, for $0 \leq \nu_m \leq \nu_0$,

$$P(\nu_a, k) = [\gamma(\nu_m)]^k M(\nu_m, k), \quad (5)$$

and

$$P(\nu_a, k) = (-1)^k [\gamma(\nu_m)]^{-k} M(-\nu_m, k), \quad (6)$$

where $M(\nu_m, k)$ is given by

$$M(\nu_m, k) = \frac{1}{2\pi} \int_0^{2\pi} M(\nu_m, \phi)e^{-jk\phi} \, d\phi, \quad (7)$$

$\nu_m^2 = \nu_a^2 + \nu_\mu^2$, $\nu_\mu = j(\sqrt{\nu_0^2 - \nu_m^2} - \nu_0)$, and $\gamma(\nu_m) = \sqrt{\nu_m^2 - \nu_\mu^2}/(\nu_m + \nu_\mu)$. We summarize the derivation (Pan, 1998b) of Eqs. (5) and (6) in the Appendix.

Equations 5 and 6 indicate that $P(\nu_a, k)$ (or, equivalently, the Radon transform of the scattering object function) can be determined from $M(\nu_m, k)$ (or, equivalently, the measured scattered data). From the estimated $P(\nu_a, k)$ (i.e., the Radon transform), one can subsequently reconstruct the scattering object function by use of computationally efficient reconstruction algorithms.

The physical origins of Eqs. (5) and (6) can be understood by examining the Fourier-space sampling pattern that is generated in a DT experiment. As the incident radiation angle $\phi$ (i.e., the orientation angle of the semicircle AOB in Fig. 2) is varied between 0 and $2\pi$, two distinct coverages of the Fourier space are generated by the two segments OA and OB of the semicircle AOB. It can readily be shown that $M(\nu_m, k)$ and $M(-\nu_m, k)$ can be obtained by use of the two distinct coverages of the Fourier space in Figures 3a and 3b, respectively.

**C. Linear Estimation of $P(\nu_a, k)$.** Because, in practice, the scattered data will contain noise (Goodman, 1986), the scattered data can be represented by a complex stochastic process $\mathbf{u}_s(\xi, \phi)$ with expected value $u_s(\xi, \phi)$. (Here and in the following, bold and normal typefaces denote a stochastic process and its expected value, respectively.) Therefore, the 2D modified FT, $\mathbf{M}(\nu_m, k)$, that is obtained from the scattered data $\mathbf{u}_s(\xi, \phi)$ is also a complex stochastic process with expected value $M(\nu_m, k)$. In the absence of noise,

both Eqs. (5) and (6) yield identical values of $P(\nu_a, k)$. When noise is present, however, the two estimates of $P(\nu_a, k)$ in Eqs. (5) and (6) are different and hence that $\mathbf{M}(\nu_m, k)$ and $\mathbf{M}(-\nu_m, k)$ contain statistically complementary information (Pan, 1998b). We will exploit this information contained in $\mathbf{M}(\nu_m, k)$ and $\mathbf{M}(-\nu_m, k)$ to achieve a bias-free variance reduction of the final estimate $\mathbf{P}(\nu_a, k)$, which generally leads to a reconstructed scattering object function with reduced variances.

A possible strategy for using the statistically complementary information inherent in $\mathbf{M}(\nu_m, k)$ and $\mathbf{M}(-\nu_m, k)$ is to form a linear combination (Pan, 1998b) of the two estimates in Eqs. (5) and (6), which is expressed as

$$\mathbf{P}(\nu_a, k) = \omega[\gamma^k \mathbf{M}(\nu_m, k)] + (1 - \omega)[(-1)^k \gamma^{-k} \mathbf{M}(-\nu_m, k)], \quad (8)$$

where $\omega$ is a weighting coefficient. Using Eqs. (5) and (6), one can show that $\mathbf{P}(\nu_a, k)$ is an unbiased estimate of $P(\nu_a, k)$. Therefore, the coefficient $\omega$ allows the two estimates in Eqs. (5) and (6) to be combined in a way that controls the variance of the final estimate $\mathbf{P}(\nu_a, k)$ without introducing any bias. Because each value of $\omega$ gives rise to a particular final estimate $\mathbf{P}(\nu_a, k)$, Eq. (8) can, in effect, be interpreted as an estimation method for obtaining $\mathbf{P}(\nu_a, k)$ (i.e., the Radon transform). Also, because, in principle, $\omega$ can have any real and/or complex value, Eq. (8) represents an infinite class of estimation methods. In this work, we will investigate the noise properties of the infinite subclass of estimation methods that arise when $\omega$ is chosen to be real in Eq. 8.

**D. Reconstruction Algorithms.** We use the FBPJ and DF algorithms to reconstruct the scattering object function from the final estimate $\mathbf{P}(\nu_a, k)$. It should be pointed out that, as will be shown below, our DF algorithm differs from conventional DF algorithms (Pan and Kak, 1983) because it only employs an explicit 1D interpolation.

*Reconstruction with the FBPJ Algorithm.* The computationally efficient FBPJ algorithm is commonly used in X-ray CT. From the estimated 1D FT, $\mathbf{P}(\nu_a, \phi_0)$, of the Radon transform, the FBPJ algorithm can be used to reconstruct the scattering object function, which is given by

$$\mathbf{a}(x, y) = \frac{1}{2} \int_0^{2\pi} \int_{-\sqrt{2}\nu_0}^{\sqrt{2}\nu_0} \mathbf{P}(\nu_a, \phi_0)|\nu_a|e^{j\nu_a\xi}\, d\nu_a\, d\phi_0, \quad (9)$$

where

$$\mathbf{P}(\nu_a, \phi_0) = \sum_{k=-\infty}^{\infty} \mathbf{P}(\nu_a, k)e^{jk\phi_0}. \quad (10)$$

The limits $\pm\sqrt{2}\nu_0$ of the integration over $\nu_a$ in Eq. (9) are determined by the highest frequency $\nu_0$ in the scattered data. This is because Eqs. (5) and (6) can only be used to estimate $P(\nu_a, k)$ for $-\sqrt{2}\nu_0 \leq \nu_a \leq \sqrt{2}\nu_0$. Physically, this corresponds to the fact that evanescent (i.e., nonpropagating) waves, which specify $M(\nu_m, k)$ for $\nu_m > \nu_0$, are not commonly utilized in DT. In our implementation of the FBPJ algorithm, an unapodized ramp filter was used. The interpolation necessary to align the backprojected data onto the discrete image matrix was performed using bilinear interpolation.

*Reconstruction with the DF Algorithm.* According to the central slice theorem, the 1D FT of the Radon transform corresponds to the 2D FT of the scattering object function $a(r, \theta)$ in a polar coordinate system. The implementation of the DF reconstruction algorithm generally involves a conversion of the samples of $\mathbf{P}(\nu_a, \phi_0)$ on a polar grid to samples of the 2D FT, $\mathbf{A}(\nu_x, \nu_y)$, of the scattering object function on a Cartesian grid, so that one can apply the inverse fast FT (FFT) to the samples of $\mathbf{A}(\nu_x, \nu_y)$ for obtaining $a(r, \theta)$. The conversion from the polar to the Cartesian grid can generally be achieved by utilizing 2D interpolation approaches such as bilinear interpolation. However, according to the central slice theorem (Barrett, 1984), $\mathbf{A}(\nu_x, \nu_y)$ can also be calculated from $\mathbf{P}(\nu_a, k)$ by use of Eq. (10) directly. In particular, when $a(r, \theta)$ is real (i.e., the scattering object is lossless), $\mathbf{A}(\nu_x, \nu_y)$ at a point $(\nu_x, \nu_y)$ on the Cartesian grids can be determined from $\mathbf{P}(\nu_a, k)$ by use of the following relationship (Metz and Pan, 1995)

$$\mathbf{A}(\nu_x, \nu_y) = \mathbf{P}(\nu_a, 0) + 2 \sum_{k=1}^{\infty} [\text{Re}\{\mathbf{P}(\nu_a, 2k)e^{j2k\psi}\}$$
$$+ \text{Im}\{\mathbf{P}(\nu_a, 2k-1)e^{j(2k-1)\psi}\}], \quad (11)$$

where $\nu_a = \sqrt{\nu_x^2 + \nu_y^2}$ and $\psi = \tan^{-1}\nu_y/\nu_x$.

Unlike 2D interpolation approaches, the calculation of $\mathbf{A}(\nu_x, \nu_y)$ by use of Eq. (11) requires only a 1D interpolation along $\nu_m$. In this work, we use Eq. (11) to obtain the samples of $\mathbf{A}(\nu_x, \nu_y)$ from the estimated $\mathbf{P}(\nu_a, k)$. The object function can then be reconstructed by inverse 2D FT of $\mathbf{A}(\nu_x, \nu_y)$, which is given by

$$\mathbf{a}(x, y) = \int\int_D \mathbf{A}(\nu_x, \nu_y)e^{j2\pi(x\nu_x + y\nu_y)}\, d\nu_x\, d\nu_y, \quad (12)$$

where $D = \{\nu_x, \nu_y | \nu_x^2 + \nu_y^2 \leq 2\nu_0^2\}$.

## III. SIMULATION STUDIES

We implemented the class of estimation methods in Eq. (8) specified by the combination coefficient $\omega$ satisfying $0 \leq \omega \leq 1$. We used computer simulation to evaluate the noise properties of images obtained by use of different combinations of the estimation methods and reconstruction algorithms.

**A. Data.** The scattering object was taken to be a lossless, uniform cylindrical disk. It was assumed that the scatterer was weakly scattering, so that the Born approximation may reasonably be taken to hold. In this way, noise in the reconstructed images can be attributed to noise in the scattered data and numerical errors, with no risk of confusion with artifacts arising from the breakdown of the weakly scattering assumption. The FDP theorem can then be used to calculate the simulated scattered data from the scattering object function (Pan and Kak, 1983).

**B. Noise Model.** To simulate the effects of a stochastic scattering object, we treated the scattered data $\mathbf{u}_s(\xi, \phi)$ as a complex stochastic process with a real and an imaginary component denoted by $\mathbf{u}_s^{(r)}(\xi, \phi)$ and $\mathbf{u}_s^{(i)}(\xi, \phi)$, respectively. Let $\mathbf{u}_s^{(r)} = u_s^{(r)} + \Delta\mathbf{u}_s^{(r)}$ and $\mathbf{u}_s^{(i)} = u_s^{(i)} + \Delta\mathbf{u}_s^{(i)}$, where $u_s^{(r)}$ and $u_s^{(i)}$ are the means of $\mathbf{u}_s^{(r)}$ and $\mathbf{u}_s^{(i)}$, respectively. The statistics of the deviates $\Delta\mathbf{u}_s^{(r)}$ and $\Delta\mathbf{u}_s^{(i)}$ are

described by a bivariate normal density function (Takai et al., 1986), which is given by

$$p(\Delta u^{(r)}, \Delta u^{(i)}) = \frac{1}{2\pi\sigma_i\sigma_r} \times \exp\left[-\frac{1}{2}\left(\frac{\Delta u^{(r)2}}{\sigma_r^2} + \frac{\Delta u^{(i)2}}{\sigma_i^2}\right)\right], \quad (13a)$$

where the constants $\sigma_r^2$ and $\sigma_i^2$ are the variances of $\Delta\mathbf{u}_s^{(r)}(\xi, \phi)$ and $\Delta\mathbf{u}_s^{(i)}(\xi, \phi)$, respectively. We also assume (Tsihrintzis and Devaney, 1993b) that the noise is uncorrelated in the $\xi$ and $\phi$ coordinates, i.e., when $\xi \neq \xi'$ and/or $\phi \neq \phi'$, the covariance

$$\mathrm{Cov}(\mathbf{u}_s(\xi, \phi), \mathbf{u}_s(\xi', \phi')) = 0. \quad (13b)$$

**C. Computer Simulations.** To study the noise properties of the reconstructed images quantitatively, we generated $N = 1,000$ sets of noisy scattered data by using the noise model in Eq. (13) with $\sigma_r = \sigma_i = 0.5$ and reconstructed 1,000 noisy images from these data sets by using different combinations of estimation methods and reconstruction algorithms. The matrix size of the reconstructed images was $128 \times 128$ pixels. The wavelength of the incident radiation was equal to 2 pixels, and the distance from the center of the scattering object to the measurement line was 200 pixels. The local image variance was calculated empirically from the $N$ sets of reconstructed images as

$$\mathrm{Var}\{\mathbf{a}(\vec{r})\} = \frac{1}{N-1}\left(\sum_{i=1}^{N}\mathbf{a}_i(\vec{r})^2 - \frac{1}{N}\left(\sum_{i=1}^{N}\mathbf{a}_i(\vec{r})\right)^2\right), \quad (14)$$

where $\mathbf{a}_i(\vec{r})$ is the $i$th image obtained with a particular combination of an estimation method and a reconstruction algorithm. The global image variance provides a convenient index for comparing the overall statistical variability of reconstructed images. The empirical global image variance, GV, was calculated by integrating the local image variance $\mathrm{Var}\{\mathbf{a}(\vec{r})\}$ over all image space, i.e.,

$$\mathrm{GV} = \int_{-\infty}^{\infty}\int_{-\infty}^{\infty}\mathrm{Var}\{\mathbf{a}(\vec{r})\}\,d\vec{r}. \quad (15)$$

(Although in this work we compare the different reconstruction algorithms using the GV, it should be noted that, from a signal detection perspective, the global variance metric may not be very useful because it does not contain information regarding the noise texture. Comparing the different reconstruction algorithms on the basis of signal detectability is beyond the scope of this study and remains a topic for future investigation.)

**D. Calculation of $M(\nu_m, k)$ and $P(\nu_a, k)$.** The 2D FT of the modified scattered data, $\mathbf{M}(\nu_m, k)$, was calculated from the measured scattered data $\mathbf{u}_s(\xi, \phi)$. For each angle $\phi$, $\mathbf{u}_s(\xi, \phi)$ was zero-padded by a factor of 2 prior to calculating $\mathbf{U}_s(\nu_m, \phi)$, resulting in a doubling of the sampling density along the $\nu_m$ axis in $\mathbf{U}_s(\nu_m, k)$ (and consequently $\mathbf{M}(\nu_m, k)$). This increase in sampling density is necessary to increase the accuracy of the interpolation of $\nu_m$ that is required for calculating $\mathbf{P}(\nu_a, k)$ from $\mathbf{M}(\nu_m, k)$ and $\mathbf{M}(-\nu_m, k)$ as described below.

The FBPJ or DF algorithm requires that $\mathbf{P}(\nu_a, \phi_0)$ be uniformly sampled on $\nu_a$. However, because of the nonlinear relationship between $\nu_a$ and $\nu_m$, the uniform sampling points at which $\nu_a$ is to be evaluated do not generally correspond to values of $\nu_m$ at which the FFT evaluates $\mathbf{M}(\nu_m, k)$. Because $\nu_m^2 = \nu_a^2 + \nu_\mu^2$, for a given value of $\nu_a$, Eq. (8) indicates that $\mathbf{P}(\nu_a, k)$ can be determined from $\mathbf{M}(\nu_m = \sqrt{\nu_a^2 + \nu_\mu^2}, k)$ and $\mathbf{M}(\nu_m = -\sqrt{\nu_a^2 + \nu_\mu^2}, k)$. In this work, we used linear interpolation to determine the values of $\mathbf{M}(\nu_m = \sqrt{\nu_a^2 + \nu_\mu^2}, k)$ and $\mathbf{M}(\nu_m = -\sqrt{\nu_a^2 + \nu_\mu^2}, k)$ from the sampled values of $\mathbf{M}(\nu_m, k)$ and $\mathbf{M}(-\nu_m, k)$.

## IV. RESULTS

From the computer simulated noiseless scattered data, we obtained two estimates of the Radon transform of the scattering object function by use of two estimation methods of Eq. (8) specified by $\omega = 0.5$ and $1.0$. From the two estimates of the Radon transform, using the FBPJ and DF algorithms, we subsequently reconstructed two scattering object functions as shown in Figures 4 and 5, respectively. The images associated with different values of $\omega$ in Figure 4 are observed to be virtually identical except for minor differences attributable to numerical errors caused by finite sampling. A similar observation can be made for the images in Figure 5 as well. The results shown in Figures 4 and 5 confirm quantitatively our assertion that the two estimates of $P(\nu_a, k)$ in Eqs. (6) and (7) (and hence their linear combinations with different $\omega$ values in Eq. 8) are identical in the absence of noise.

Using the computer simulated noisy scattered data, we obtained two estimates of the Radon transform of the scattering object function by use of two estimation methods of Eq. (8) specified by $\omega = 0.5$ and $1.0$. From the two estimates of the Radon transform, using the FBPJ and DF algorithms, we subsequently reconstructed the two noisy scattering object functions shown in Figures 6 and 7. The images associated with different values of $\omega$ in Figure 6 are observed to be clearly different from each other. A similar observation can be made for the images in Figure 7 as well. Therefore, the results in Figures 6 and 7 confirm quantitatively our assertion that the two estimates of $P(\nu_a, k)$ in Eqs. (6) and (7) (and hence their linear combinations with different $\omega$ values in Eq. 8) respond to noise differently. Also, different reconstruction algorithms propagate noise and numerical errors differently. This can be verified, for example, by observation of the conspicuous differences between the noiseless images in Figures 4a and 5a and between the noisy images in Figures 6a and 7a for $\omega = 0.5$.

Figure 8 displays empirical image-variance profiles calculated from noisy images obtained from 1,000 sets of computer simulated noisy scattered data. The solid and dotted curves show the variance profiles calculated from noisy images that were reconstructed with the DF algorithm from 1,000 sets of estimates of the Radon transform by use of the estimation methods specified by $\omega = 0.85$ and $0.5$, respectively. The dashed and dashed-dotted curves show the variance profiles of noisy images reconstructed with the FBPJ algorithm from 1,000 sets of estimated Radon transforms by use of the estimation methods specified by $\omega = 0.85$ and $0.5$, respectively. It is seen from Figure 8 that the variances of images associated with $\omega = 0.5$ are smaller than those of the images associated with $\omega = 0.85$ for both reconstruction algorithms. As we already observed in Figures 3 and 4, for both values of $\omega$, the variances of the images reconstructed by the DF algorithm are higher than those of the images reconstructed by the FBPJ algorithm. Qualitatively similar results were also obtained for different values of $\omega$ and different noise-model parameters $\sigma_r$ and $\sigma_i$. This is explained by the well-known
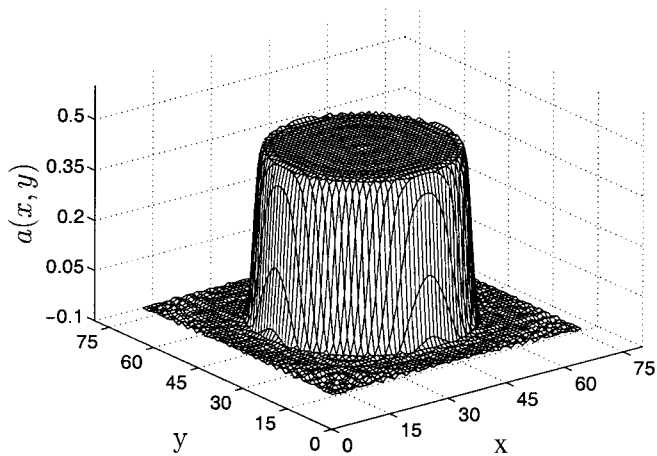
(a)
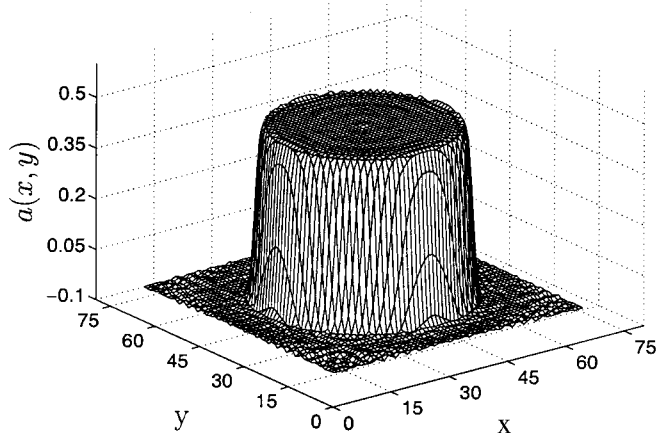


(b)

**Figure 4.** Noiseless images of a lossless cylindrical scattering object function obtained by using the (a) $\omega = 0.5$ and (b) $\omega = 1.0$ estimation methods with the FBPJ reconstruction algorithm.

fact that the DF algorithm is more sensitive to noise and numerical errors than is the FBPJ algorithm (Anastasio et al., 1998).

We calculated sets of 1,000 estimated Radon transforms by use of several estimation methods specified by values of $\omega \in [0, 1]$. From each set of estimated Radon transforms, sets of images were reconstructed by use of the FBPJ and DF reconstruction algorithms. Therefore, for images obtained using each reconstruction algorithm (DF or FBPJ), the global image variance can be interpreted as a function of $\omega$. Figures 9a and 9b display the global image variances as functions of $\omega$ calculated from images obtained by use of the FBPJ and DF reconstruction algorithms, respectively. The curves in Figure 9 indicate that, for each reconstruction algorithm, different global image variances are obtained when different estimation methods are used to estimate the Radon transform. Figure 9 reveals that

the estimation method with $\omega = 0.5$ produces images that have smaller global image variance than any other estimation method in the class. This observation is in agreement with the theoretical predictions made in Pan (1998b), where it was proved analytically that, for uncorrelated data noise (see Eq. 13b), $\omega = 0.5$ determines the optimal estimation method that yields the smallest global image variance. In addition, it was predicted [23] that the global image variance is a parabolic function of $\omega$ and that the ratio between the maximum and minimum global image variances is $\frac{1}{2}$. These theoretical predictions are verified by the results in Figures 9a and 9b.

## V. DISCUSSION

It is known that the measured scattered data in DT with the classical scan geometry provide two distinct sets of samples of the FT of the
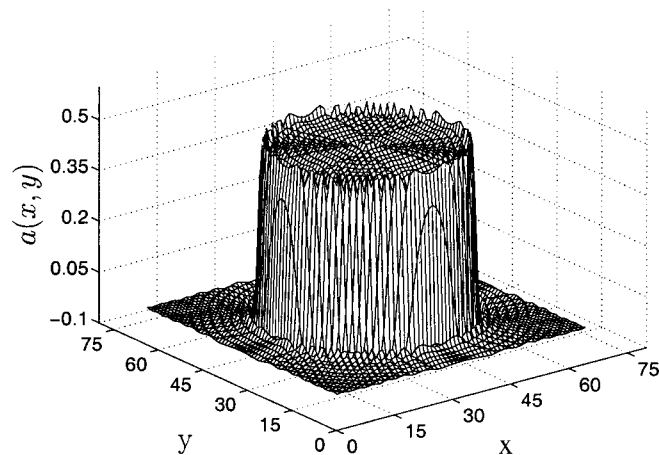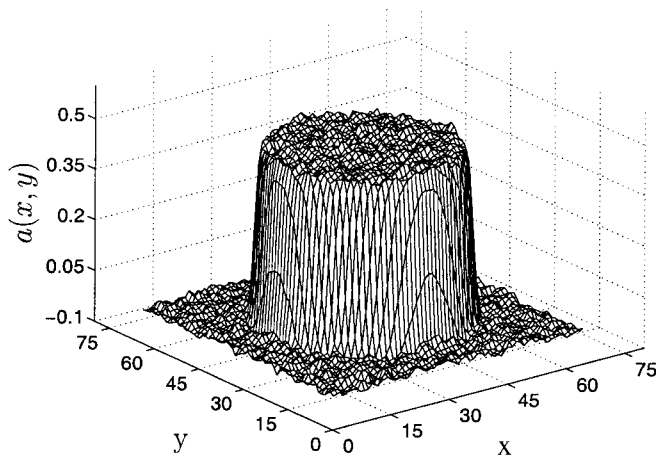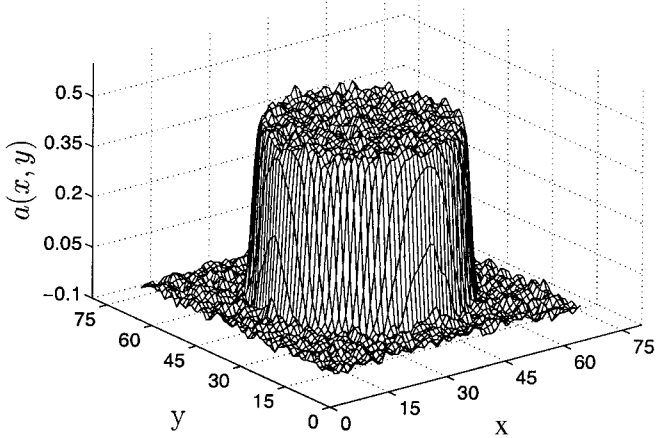


(a)
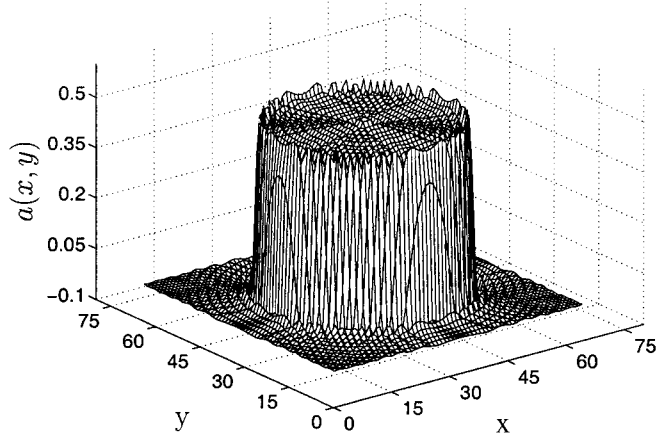


(b)

**Figure 5.** Noiseless images of a lossless cylindrical scattering object function obtained by using the (a) $\omega = 0.5$ and (b) $\omega = 1.0$ estimation methods with the DF reconstruction algorithm.
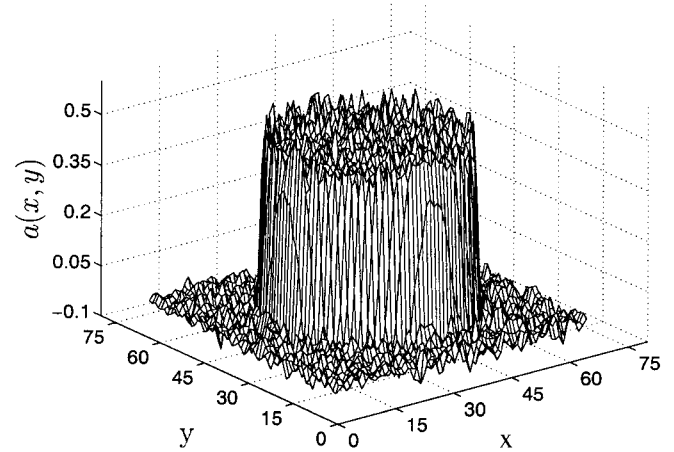
obtaining the Radon transform of the scattering object function from the scattered data in DT.

We have implemented the estimation methods in this infinite class and investigated the noise properties of these estimation methods and the FBPJ and our DF reconstruction algorithms by using a large number of computer simulated scattered data sets. The numerical results corroborated the theoretical assertions, demonstrating that the estimation methods propagate noise in the scattered data differently and that the noise properties of the reconstructed images depend on the choice of estimation methods and reconstruction algorithms. Through our simulation studies, we have demonstrated that it is possible to achieve a bias-free reduction of the statistical variation in the reconstructed scattered object function by utilizing complementary statistical information inherent in the scattered data.



(a)



(b)

**Figure 6.** Noisy images of a lossless cylindrical scattering object function obtained by using the (a) $\omega = 0.5$ and (b) $\omega = 1.0$ estimation methods with the FBPJ algorithm.
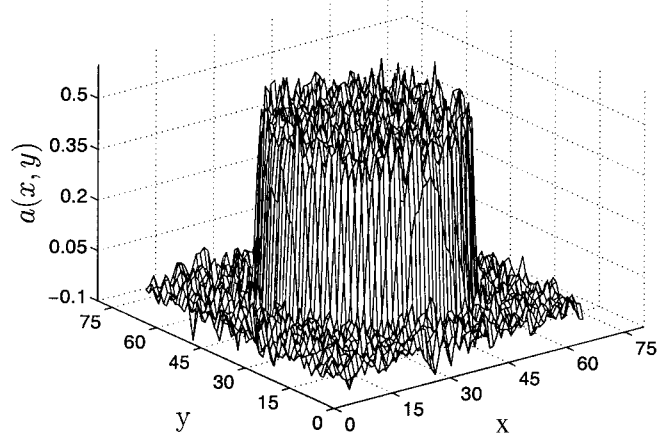
scattering object function (Pan and Kak, 1983; Devaney, 1982). In principle, the scattering object function can be reconstructed from either of these two distinct sets of samples. Using the conventional DF algorithm, one often reconstructs the scattering object function from only one set of the samples, simply discarding the other set (Pan and Kak, 1983; Gelius et al., 1991). However, we showed that, in the presence of data noise, the two sets of samples contain statistically complementary information and that this information can be used to achieve a bias-free reduction of variance in the reconstructed scattering object function. In an attempt to make use of this information, we introduced a linear combination of the knowledge derived from the two sets of samples, which leads to the development of an infinite class of estimation methods (Eq. 8) for



(a)



(b)

**Figure 7.** Noisy images of a lossless cylindrical scattering object function obtained by using the (a) $\omega = 0.5$ and (b) $\omega = 1.0$ estimation methods with the DF algorithm.
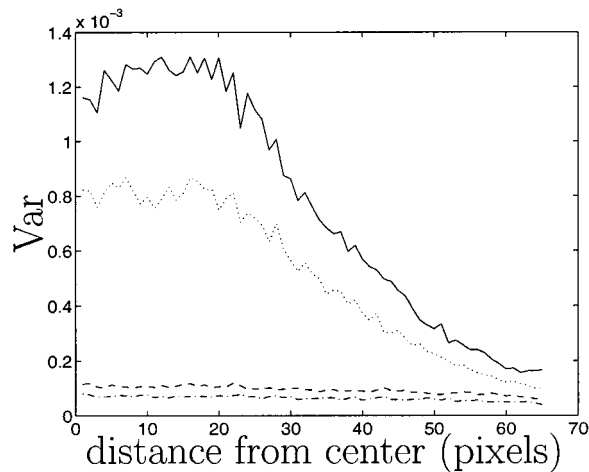
**Figure 8.** Variances calculated from images obtained by using the $\omega = 0.5$ estimation method with the DF reconstruction algorithm (dotted line) and the FBPJ reconstruction algorithm (dashed-dotted line) and by using the $\omega = 0.85$ estimation method with the DF reconstruction method (solid line) and the FBPJ reconstruction method (dashed line). The variances obtained using the $\omega = 0.5$ estimation method are smaller than those associated with the $\omega = 0.85$ estimation method for both the FBPJ and DF reconstruction algorithms.

(The use of an explicit smoothing operation generally introduces bias in the reconstructed scattering object function.)

Single-photon-emission-computed tomography (SPECT) is a medical imaging modality that collects $\gamma$-rays emitted from radioactive isotopes that are administered to the object (Metz and Pan, 1995). The emitted $\gamma$-rays are subject to attenuation before measurement. From the measured attenuated projections, the distribution of the isotopes in the object can be reconstructed. It is interesting to note that despite the fact that SPECT with uniform attenuation and DT are two imaging modalities that are based on very different physical processes, the mathematics and statistical analyses of the image reconstructions are virtually identical. For example, it can be shown that the 2D FT of the measured data in SPECT with uniform attenuation is related to $P(\nu_a, k)$ by equations completely analogous to those derived for DT (Eqs. 5 and 6). As for the DT problem, infinite classes of methods for estimating the Radon transform in SPECT are obtained by forming different linear combinations of the two estimates $P(\nu_a, k)$. For a detailed comparison of the SPECT and DT reconstruction problems, see Pan (1998a).

In this work, we implemented and evaluated the estimation methods. In particular, we investigated the noise properties of the estimation methods with real-valued $\omega$. It can be shown, however, that the optimal $\omega$ that minimizes the variance of the final estimate $\mathbf{P}(\nu_a, k)$ is a complex function of $\nu_m$ and $k$. The noise properties of estimation methods with $\omega$ being a complex function of $\nu_m$ and $k$ require further investigation. It was shown [23] that, for a family of estimation methods index with $\omega(\nu_m, k)$, where $\omega(\nu_m, k) + \omega(-\nu_m, k) = 1$, there exists a corresponding family of generalized FBPP reconstruction algorithms. The well-known FBPP algorithm proposed by Devaney (1982) can be interpreted as a special member of the GFBPP family with $\omega = \frac{1}{2}$. Extension of the current work to 3D DT and 2D DT with nonclassical imaging geometries is under way and will be reported elsewhere.

## APPENDIX: DERIVATION OF THE RELATIONSHIP BETWEEN $P(\nu_a, k)$ AND $M(\nu_m, k)$

For completeness, we outline the derivation (Pan, 1998b) of the relationship between $P(\nu_a, k)$ and $M(\nu_m, k)$. Using Eq. (3) and noticing $\xi = r \cos(\phi_0 - \theta)$, the 1D FT of the Radon transform $p(\xi, \phi_0)$ is given by
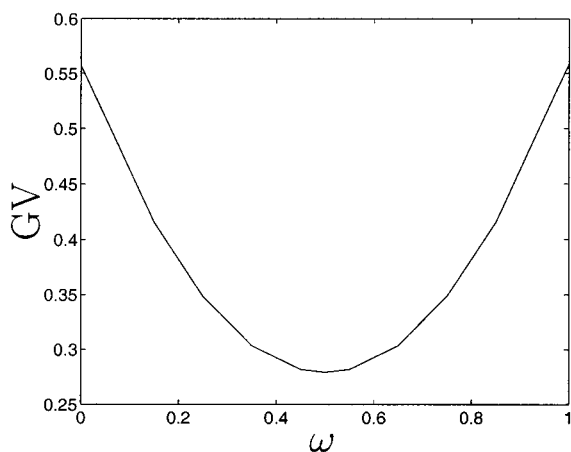


(a)
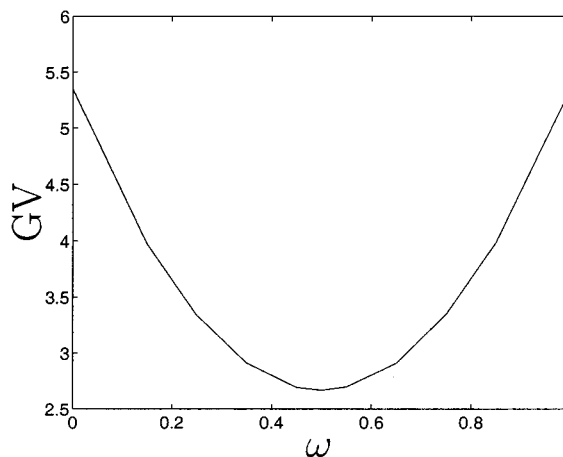


(b)

**Figure 9.** Global image variances as functions of $\omega$ for (a) the FBPJ reconstruction algorithm and (b) the DF reconstruction algorithm. For the uncorrelated noise model in Eq. (13b), both reconstruction algorithms produce the minimum global image variances at $\omega = 0.5$.

$$P(\nu_a, \phi_0) \equiv \int_{\xi=-\infty}^{\infty} p(\xi, \phi_0) e^{-j2\pi\nu_a\xi} \, d\xi$$

$$= \int_{\theta=0}^{2\pi} \int_{r=0}^{\infty} a(\vec{r}) e^{-j2\pi\nu_a r \cos(\phi_0-\theta)} r \, dr \, d\theta. \quad \text{(A1)}$$

We now turn to Eq. (2), which, for $|\nu_m| \le \nu_0$, can be rewritten as

$$M(\nu_m, \phi) = \int_{-\infty}^{\infty} \int_{-\infty}^{\infty} a(\vec{r}) \exp[-j2\pi\sqrt{\nu_m^2 + (\nu'-\nu_0)^2} r \cos(\phi$$
$$+ \phi' - \theta)] \, d\vec{r}, \quad \text{(A2)}$$

where

$$\cos\phi' = \frac{\nu_m}{\sqrt{\nu_m^2 + (\nu'-\nu_0)^2}} \text{ and } \sin\phi' = \frac{\nu'-\nu_0}{\sqrt{\nu_m^2 + (\nu'-\nu_0)^2}}. \quad \text{(A3)}$$

Comparison of Eqs. (A1) and (A2) yields the relationship

$$P(\nu_a, \phi_0) = M(\nu_m, \phi), \quad \text{(A4)}$$

where

$$\phi = \phi_0 - \phi' \quad \text{(A5)}$$

and

$$\nu_m^2 = \nu_a^2 \left[ 1 - \left( \frac{\nu_a}{2\nu_0} \right)^2 \right]. \quad \text{(A6)}$$

The 1D Fourier series expansions of $P(\nu_a, \phi_0)$ and $M(\nu_m, \phi)$ are defined as

$$P(\nu_a, k) \equiv \frac{1}{2\pi} \int_{\phi_0=0}^{2\pi} P(\nu_a, \phi_0) e^{-jk\phi_0} \, d\phi_0 \quad \text{(A7)}$$

and

$$M(\nu_m, k) \equiv \frac{1}{2\pi} \int_{\phi=0}^{2\pi} M(\nu_m, \phi) e^{-jk\phi} \, d\phi, \quad \text{(A8)}$$

respectively. For simplicity, we refer to $P(\nu_a, k)$ and $M(\nu_m, k)$ as the 2D FTs of the Radon transform and modified data function, respectively. Using Eqs. (A4) and (A5) in Eq. (A7) yields

$$P(\nu_a, k) = \frac{1}{2\pi} \int_{\phi=0}^{2\pi} M(\nu_m, \phi) e^{-jk(\phi+\phi')} \, d\phi = \gamma(\nu_m)^k M(\nu_m, k), \quad \text{(A9)}$$

where $\gamma(\nu_m) = e^{-j\phi'} = \sqrt{\nu_m^2 - \nu_\mu^2}/(\nu_m + \nu_\mu)$ with $\nu_\mu = j(\sqrt{\nu_0^2 - \nu_m^2} - \nu_0)$. It can be shown that $\gamma(-\nu_m) = -\gamma(\nu_m)^{-1}$.

Notice that for a given real value of $\nu_a$ satisfying $0 \le \nu_a \le 2\nu_0$, there are two values of $\nu_m$ that satisfy Eq. (A6):

$$\nu_{m+} = -\nu_{m-} = \nu_m = \nu_a \sqrt{1 - \frac{\nu_a^2}{4\nu_0^2}} \quad \text{(A10)}$$

Substitution of $\nu_{m+}$ and $\nu_{m-}$ into Eq. (A9) yields the two estimates of $P(\nu_a, k)$ in Eqs. (5) and (6):

$$P(\nu_a, k) = [\gamma(\nu_m)]^k M(\nu_m, k) \quad \text{(A11)}$$

$$= (-1)^k [\gamma(\nu_m)]^{-k} M(-\nu_m, k). \quad \text{(A12)}$$

## REFERENCES

M. Anastasio, M. Kupinski, and X. Pan, Noise properties of reconstructed images in ultrasound diffraction tomography, IEEE Trans Nuclear Sci 45 (1998), 2216–2223.

M.P. Andre, P.J. Martin, G.P. Otto, L.K. Olson, T.K. Barrett, B.A. Apivey, and D.A. Palmer, A new consideration of diffraction computed tomography for breast imaging, Acoustical Imaging 21 (1995), 379–390.

H.H. Barrett, The Radon transform and its applications, Prog Optics 21 (1984), 219–286.

L. Chernov, Wave propagation in random media, McGraw-Hill, New York.

W. Chew and Y. Wang, Reconstruction of two-dimensional permitivity distribution using the distorted born iterative method, IEEE Trans Med Imaging 9 (1990), 218–225.

A. Devaney, A filtered backpropagation algorithm for diffraction tomography, Ultrasonic Imaging 4 (1982), 336–350.

D.G. Fischer and E. Wolf, Theory of diffraction tomography for quasi-homogeneous random objects, Optics Commun 133 (1997), 17–21.

L. Gelius, I. Johansen, N. Sponheim, and J. Stamnes, Diffraction tomography applications in medicine and seismics, NATO advanced workshop on inverse problems in scattering and imaging, North Falmouth, MA, 1991.

J. Goodman, A random walk through the field of speckle, Optical Eng 25 (1986), 610–612.

P. Grassin, B. Duchene, and W. Tabbara, "Diffraction tomography: some applications and extension to 3-d ultrasound imaging," Mathematical methods in tomography, Springer-Verlag, Heidelberg, 1991, 98–105.

G. Heidbreder, Multiple scattering and the method of Rytov, J Optical Soc Am 57 (1967), 1477–1479.

A. Ishimaru, Wave propagation and scattering in random media, Academic, New York, 1978.

S. Johnson and M. Tracy, Inverse scattering solutions by a sinc basis, multiple source, moment method—part i: theory, Ultrasonic Imaging 5 (1983a), 361–375.

S. Johnson and M. Tracy, Inverse scattering solutions by a sinc basis, multiple source, moment method—part ii: numerical evaluations, Ultrasonic Imaging 5 (1983b), 376–392.

M. Kaveh, M. Soumekh, and J. Greenleaf, Signal processing for diffraction tomography, IEEE Trans Sonics Ultrasonics 31 (1984), 230–239.

G. Kino, Acoustic imaging for nondestructive evaluation, Proc IEEE 67 (1979), 510–525.

K. Langenberg, Digital ultrasonic imaging, Proc 11th World Conf Nondestructive Testing, 1985, Las Vegas, NV.

C. Lu, W. Chew, and G. Otto, Image reconstruction with acoustic measurement using distorted born iterative method, Ultrasonic Imaging 18 (1996), 140–156.

C.E. Metz and X. Pan, A unified analysis of exact methods of inverting the 2-d exponential radon transform, with implications for noise control in spect, IEEE Trans Med Imaging 14 (1995), 643–658.

P.M. Morse and K.U. Ingard, Theoretical acoustics, Princeton University Press, Princeton, NJ, 1986.

R. Mueller, M. Kaveh, and G. Wade, Reconstructive tomography and applications to ultrasonics, Proc IEEE 67 (1979), 567–587.

S. Pan and A. Kak, A computational study of reconstruction algorithms for diffraction tomography: interpolation versus filtered backpropagation, IEEE Trans Acoustics Speech Signal Processing 31 (1983), 1262–1275.

X. Pan, Analysis of 3d spect image reconstruction and its extension to ultrasound diffraction tomography, IEEE Trans Nuclear Sci 45 (1998a), 1308–1316.

X. Pan, A unified reconstruction theory for diffraction tomography with considerations of noise control, J Optical Soc Am 15 (1998b), 2312–2326.

E. Robinson, Image reconstruction in exploration geophysics, IEEE Trans Sonics Ultrasonics 31 (1984), 259–270.

D. Rouseff and R. Porter, Diffraction tomography and the stochastic inverse scattering problem, J Acoustical Soc Am 89 (1991), 1599–1605.

N. Takai, H. Kadono, and T. Asakura, Statistical properties of the speckle phase in image and diffraction fields, Optical Eng 25 (1986), 627–635.

G. Tsihrintzis and A. Devaney, Stochastic diffraction tomography: theory and computer simulation, Signal Processing 93 (1993a), 49–64.

G.A. Tsihrintzis and A.J. Devaney, Application of a maximum likelihood estimator in an experimental study in ultrasonic diffraction tomography, IEEE Trans Med Imaging 12 (1993b), 545–554.